IEEE Access
Multidisciplinary ⋮ Rapid Review ⋮ Open Access Journal

Received 29 August 2023, accepted 24 September 2023, date of publication 28 September 2023,
date of current version 11 October 2023.

Digital Object Identifier 10.1109/ACCESS.2023.3320275

RESEARCH ARTICLE

Force Equalization Control of Redundant Electromechanical Actuation System by FOPID and Current Feedforward

JIANZHONG YANG, DONG HOU, XIAOZHE SUN, AND JINPENG ZUO
College of Safety Science and Engineering, Civil Aviation University of China, Tianjin 300300, China
Corresponding author: Xiaozhe Sun (sxz_2002@163.com)

This work was supported in part by Civil Aviation University of China Graduate Research Innovation Grant 2021YJS076.

ABSTRACT To solve force-fight problem of the fly-by-wire redundant electromechanical actuation system(EMAs) in an active-active mode, a force equalization control method with feedforward and feedback control is proposed. Aiming at the un-ideal stability and robust performance of force equalization controller, an optimized Fractional Order PID controller with current feedforward (FO+IF)is adopted. Aiming at the limitation of traditional parameter tuning, the controller parameters are optimized iteratively using the particle swarm optimization (PSO) algorithm. To improve the anti-interference performance of the system, a state observer for load torque is introduced into the current feedforward control. Through setting a serious force fight situation with multiple disturbances, the performance of FOPID and FO+IF on force fight and position response were compared, and the robustness of the system under the influence of sensitive parameters was analyzed by Monte Carlo method. The experimental results show that FO+IF can effectively improve the impact of static force fight and dynamic force fight on the system.

INDEX TERMS Redundant actuator, electromechanical actuators, force fight, fractional order controller, particle swarm optimization, current feedforward, force equalization.

I. INTRODUCTION

As the concept of more-electric aircraft remains to expand and develop in the aviation field, the flight control system expects to substitute many secondary energy systems such as hydraulic, pneumatic, and mechanical actuators with electric actuators which are environmentally friendly, small in size, and easy to maintain [1], [2]. More and more civil aircraft subsystems such as brake systems, flight control systems, aircraft environment control systems, aircraft anti-icing systems, and other systems choose electro-mechanical actuators (EMA) as their primary driving component. One of the crucial issues in more-electric aircraft flight control actuation systems is to develop of electro-mechanical actuators with good performance and high safety [3], [4]. To fulfill the safety requirements of FAR25.1309 airworthiness regulations for a flight control system with extremely low failure probability, modern civil aircraft flight control surfaces are generally arranged with a redundant configuration of two or more actuators, and the surfaces are driven in the active-active working mode [3]. There is a serious force fight in the dual redundant electromechanical actuation system performing in active-active mode: The electromechanical actuation system is a complicated system with high stiffness, strong coupling, and nonlinearity, in the system response, the dynamic response characteristics of the two actuators acting together on the surface are different, and there is always an output torque imbalance called force fight, which will adversely affect the surface stability and system power, the long-term force fight may even lead to fatigue failure problem, decreasing the payload of the actuation system and even resulting in airfoil fatigue affecting the flight safety [5]. This puts forward higher requirements for force fight control method of the electromechanical actuation system in active-active mode.

To ensure the reliability of the redundant electromechanical actuation system, it is essential to compensate for the

The associate editor coordinating the review of this manuscript and approving it for publication was M. Venkateshkumar.

force fight on the servo reaction of the actuation system [6]. Currently, the control methods for force fight are mainly composed of structural compensation and force equalization control [7], [8]. Typically used force compensation methods take the difference between the output forces of the two actuators and then introduce it into the feedback channel to minimize the difference between the two actuators, realizing the force fight mitigation [9], [10], [11], [12], [13].

Many scholars have applied controllers for force equalization, among which Zhang [14] of WIU in 2014 proposed a PID feedback method to compensate for the position signal, and force fight of the dynamic response process was significantly reduced. 2019 Salman et al of Beihang University [15] [16] based on force fight problem of a dissimilar redundant actuation system, used the least squares method to transform the nonlinear system into a linear system, applied linear matrix inequalities (LMIs) to design disturbance observers and controllers, which have good control effect for external load disturbance signals, but state observers can only compensate for limited types of disturbances. In 2020, XUE from Shanghai Jiao Tong University [17] proposed a set of force equalization algorithms based on the pressure difference and position compensation feedback and validated the control method on the Iron Bird platform. WU Rehman [18] from the University of Science and Technology Beijing 2021 designed a fractional-order PID feedback controller based on a linear simulation model of a non-similar residual system, but only verified force fight in the case of external load perturbation. SUN [19] proposed a force equalization method based on the combined action of speed and acceleration feedforward compensation control and PID feedback control in 2022, but the method is designed based on friction and motor linear parameters, the selection of controller parameters is subjective.

In above studies, only force fight caused by external load changes is considered when designing the control algorithm. In practice, force fight is not only caused by load changes, but also caused by interference and parameter fluctuations [20], [21], [22]. Above control methods can reduce force fight in a dynamic process to meet control requirements, to enhance the fault tolerance ability of the system, but the force equalization controller should also be designed to meet the accuracy of the position servo system [23]. In 2018, Robert Kowalski [33] of the German Aerospace Center proposed a force fight compensation method that includes a feedback loop containing an optimal linear secondary output regulator (LQR) and a feed-forward controller based on a general regression neural network (GRNN), but the accuracy of neural networks has a lot to do with training samples, and is more complex and computationally intensive. In 2019, LI [34] of Northwestern Polytechnical University proposed a nonlinear controller combining adaptive control and observer-based interference suppression control to solve the master-main mode control problem of digital reference adaptive system under internal leakage fault, large disturbance and force fight problems. Among them, the internal leakage fault is adapted by a simple reconstruction strategy based on online adaptation of fault parameters, and the effectiveness of the proposed control algorithm is finally proved by comparing the simulation results. However, the adaptive control algorithm has a high dependence on the model, and the online adaptive control system is more complex.

The parameters of controller obtained by manually tuning the controller parameters can use optimization algorithms to improve control quality. Due to the high reliability and fault-tolerance requirements, a PID force equalization controller cannot meet the requirements of system robustness and high accuracy to a certain extent. The accuracy and precision of the force equalization controller can still be improved.

Aiming at improving control effect and accuracy of force equalization controller, this paper chooses a combination of fractional-order force equalization feedback control method with particle swarm optimization (PSO) and feedforward compensation controller. While considering the system response accuracy and minimizing force fight to meet control requirements, the control effect is improved.

II. FORCE FIGHT OF THE REDUNDANT ELECTROMECHANICAL SYSTEM

A. MODELING OF ELECTROMECHANICAL SYSTEM

The dual redundant electromechanical actuation system consists of a controller, drive circuit, brushless DC motor, sensor, mechanical transmission device, surface, etc. The schematic diagram of the dual redundant electromechanical actuation principle is shown in Figure 1. The output force of these two actuators acts on the surface together.

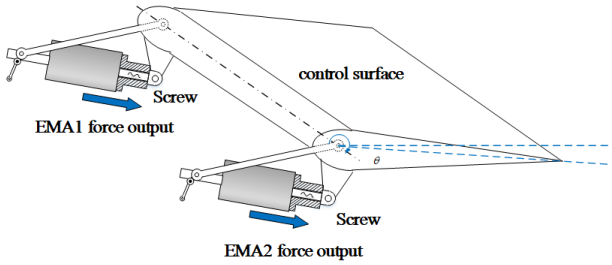

FIGURE 1. Schematic diagram of redundant electromechanical system.

Under ideal conditions, the relationship between the internal voltage and current of the motor ideally can be equivalent to equation (1). Where R_a and L_a is Equivalent resistance and equivalent inductance, k_e is back EMF Constant.

$$\mathrm{U_d} = \mathrm{R_a I} + \mathrm{L_a}\frac{\mathrm{di}}{\mathrm{dt}} + \mathrm{k_e}\omega \tag{1}$$

The equation of electromagnetic torque of brushless DC motor is in equation (2). e_a, e_b, e_c denote the winding counter-electromotive force of each phase, phase currents, ω is motor rotation speed, T_e is motor electromagnetic torque.

$$\mathrm{T_e} = (\mathrm{e_a i_a} + \mathrm{e_b i_b} + \mathrm{e_c i_c})/\omega \tag{2}$$

The equation of motion of BLDC is as in equation (3). B is damping factor, J is motor inertia, T_l is load torque, T_f is

frictional torque.

$$T_e = T_l + T_f + B\omega + J\frac{d\omega}{dt} \tag{3}$$

The motor internal control loop consists of current loop, speed loop and position control loop. The rotational displacement output after position control is converted into horizontal displacement by screw and gearbox, which drives the surface to deflect. The output displacement θ_n is proportional to the screw output angle θ_g after the deceleration device. The screw gearbox can be approximated as equation (4), thereinto K_x is the screw reduction ratio.

$$\theta_g = K_x \cdot \theta_n \tag{4}$$

If the inertia of the rudder surface itself is ignored, the linear output displacement X_a of the ball screw and the output angle of the ball screw are approximately equivalent to the proportional relationship, such as equation (6). The coefficient K_a is related to the diameter of the ball screw as well as the motor characteristics.

$$x_a = K_a \cdot \theta_g \tag{5}$$

The flight control system will be subjected to changing flight loads at all times during operation, surface will be equated to the inertial load system as in equation(6). x_a is linear output displacement, x_L is surface deflection displacement. M_{cs} represents the equivalent mass of the rudder surface, B_{cs} is the damping coefficient of rudder surface, K_d is rudder surface stiffness factor, F_i is motor output driving force, K_{ms} is connection stiffness, the relationship between rudder deflection angle θ and displacement x_L can be equated as a proportional relationship, which scale factor is the radius of rotation of the rudder surface R_{cs}.

$$F_i = M_{cs}\ddot{x}_L + B_{cs}\dot{x}_L + K_d x_L \tag{6}$$

$$F_i = K_{ms}(x_a - x_L) \tag{7}$$

According to the above equation, the system simulation model is completed. A step position command with an amplitude of 5° at 0.2 Hz was applied to the system, the open-loop frequency response of the system is measured [23] to prove the system stability.

According to the criterion of system frequency stability in the automatic control principle, the margin is positive and the system is stable. The higher the margin, the stronger the system stability. The open-loop frequency domain response of the position loop is shown in Figure 2. The amplitude margin is 38.1dB, the phase margin is 90.2 °, and the system is stable.

B. ANALYSIS OF FORCE FIGHT

Force fight is obtained as in equation (8), ΔF_d represents the uncertainties that cause force fight in the flight control system, such as: transmission intervals, transmission friction, delay in signal transmission loop, noise, etc. F_{ff} is difference in force between the two actuators, K_{ms1}, K_{ms2} is two actuator connection stiffness.

$$F_{ff} = K_{ms1}(x_{a1} - x_L) + K_{ms2}(x_{a2} - x_L) + \Delta F_d \tag{8}$$

The output displacement difference between the two actuators is the main cause of the system force fight [25], and several types of factors that have the greatest impact on force fight of the electromechanical actuator system are shown in Table 1.

The above factors are injected into the dual redundant electromechanical actuators to obtain the worst force fight situation of the system. Dynamic force fight is defined as force fight generated during the dynamic process before the system reaches a steady state, and the peak of force fight usually occurs during the dynamic process; the static force fight represents force fight that still exists in the system after the position response reaches steady state. Dynamic force fight can reach 145961N, static force fight is about 52561N under the action of each influencing factor.

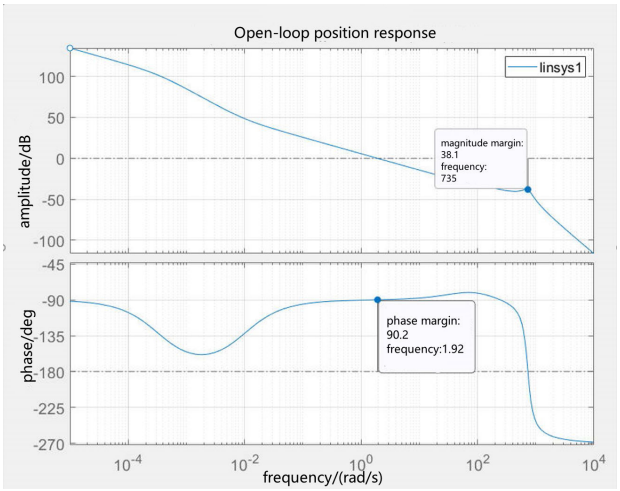

FIGURE 2. Frequency domain characteristics of EMA.

TABLE 1. Influencing parameters of force fight.

Influencing Factors	Model presentation
Position Offset	2% increase in input position signals to individual actuators in 0.4 seconds
Position Command Offset	2% increase in input position commands to individual actuators in 0.4 seconds
Position signal intermittent	Single actuator position signal with 0.01s interruption at 0.2s
white noise	Transmission components have a 50hz noise with an amplitude of 0.2% of the position signal
friction	There is a 30% difference in the friction of the motor drive section
transmission backlash	200% increase in backlash to the gearbox of a single actuator
transmission stiffness	25% increase in actuator stiffness
transmission efficiency	15% reduction in transmission efficiency of a single actuator
load torque	5000N increase in load torque to individual actuators in 0.1 seconds

III. INTRODUCTION OF FEEDFOWARD AND FEEDBACK CONTROL

A. INTRODUCTION OF FORCE EQUALIZATION CONTROL STRATEGY

The block diagram of the dual redundancy actuators force equalization control is shown in Figure 3. A control strategy that combines feedforward and feedback control is selected combining the advantages of force fight control and system immunity to interference. Position lag introduced by feedback is compensated by feedforward, while the disadvantage that feedforward control can only compensate for a few specific types of disturbances is improved by feedback [26].

The position response deviation and force fight are used as feedback inputs to the controller, and the feedback position compensation is generated by the feedback controller to compensate for the position controller of the two electromechanical actuators. The parameters of the controller are iteratively calculated by the optimization algorithm. The feedforward control designs a state observer according to the known speed and current parameters to accurately observe the external torque of the system, and then compensates the external torque of the system to the current signal of the motor in advance.

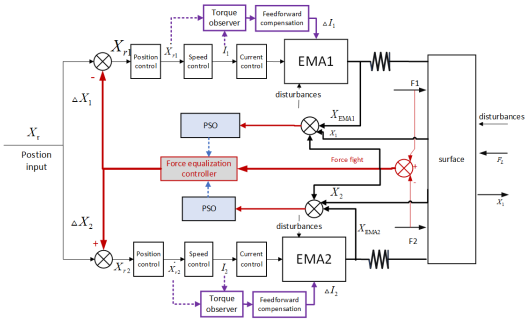

FIGURE 3. FOPID controller parameter optimized by PSO and current feedforward controller.

The red line in the figure represents the feedback controller, while the purple line represents the feedforward controller. In the force equalization controller, PSO and FOPID methods are used to improve the performance of the feedback controller, which combined with current feedforward is to improve the anti-interference performance of the system.

B. DEFINITION OF FRACTIONAL ORDER CALCULUS

In order to better explain the mathematical meaning of fractional order calculus, an operator of fractional order calculus ${}_{t0}\vartheta_t^{\alpha}$ is introduced as equation (9), where α is real numbers and t is an independent variable.

The block diagram of the fractional order PID control system is shown in Fig 4. Fractional order PID expands the integer order to the fractional domain, and adds two adjustable parameters, integral order λ and differential order μ, the integral order indicates the strength of the integral effect. The appropriate integration order makes the system have a smaller stable tolerance, higher accuracy of dynamic response, and better medium frequency bandwidth of amplitude-frequency characteristics [27], [28].

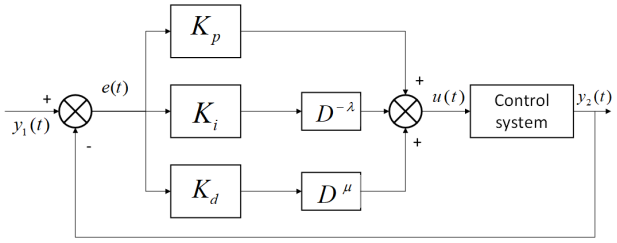

FIGURE 4. Fractional order PID control diagram.

The formula for PID can be approximated as Equation 7. ${}_{t0}\vartheta_t^{\alpha}$ is the introduced fractional calculus operator, where α is limited to real numbers and t is the independent variable.

$$ {}_{t0}\vartheta_t^{\alpha} f(t) = \begin{cases} \dfrac{d^{\alpha}}{dt^{\alpha}} f(t), & \alpha > 0 \\ f(t), & \alpha = 0 \\ \displaystyle\int_t^{t_0} f(\tau) d\tau^{-\alpha}, & \alpha < 0 \end{cases} \tag{9} $$

Fractional order PID extends the integer order to the fractional domain, and adds two adjustable parameters, integral order λ and differential order μ. The lower-upper frequency of FOPID is 10^{-4} and 10^{4}, the filter order is usually set to 5.

The approximation of fractional order in the control system is shown in Figure 5, using a set of zero-pole folds from the integer order to approximate the linear properties of the frequency of the fractional order calculus, which can reduce steady-state error, improve accuracy of dynamic response and medium frequency bandwidth of amplitude-frequency characteristics.

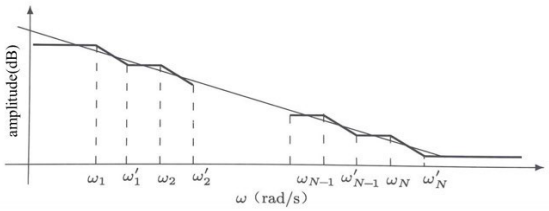

FIGURE 5. Segmented folding approximation of FOPID.

The application of fractional-order PID to force equalization is conducive to improving the rapidity of the controller, reducing the peak of force fight in response process, and also reducing the steady-state error of force fight and improving the stability of the system.

C. PRINCIPLE OF PARTICLE SWARM PARAMETER OPTIMIZATION

The particle swarm algorithm was chosen as the optimization algorithm for the system force equalization controller [29]. The particle swarm is initialized as a group of random particles, and in each iteration, the particles are continuously

updated through individual extremes and global extremes to produce a new generation of the population [30].

Defined for the "i" th particle in the particle population in n-dimensional space, $x^i(k) = [x_1^i \ x_2^i \ \dots \ x_n^i]^T$ denotes the current position of the particle. $p^i(k) = [p_1^i \ p_2^i \ \dots \ p_n^i]^T$ indicates that the particle has optimal fitness $f_p^i(k)$, the optimal position of the population particle is denoted as $p^g(k) = [p_1^g \ p_2^g \ \dots \ p_n^g]^T$, $v^i(k) = [v_1^i \ v_2^i \ \dots \ v_n^i]^T$ is the search direction of the particle. Updated speed and position can be expressed as equation (10).

$$\begin{cases} x_j^i(k+1) = x_j^i(k) + v_j^i(k+1) \\ v_j^i(k+1) = \omega(k) v_j^i(k) + \varphi_1 \mathrm{rand}(0, a_1)(p_j^i(k) - x_j^i(k)) \\ \qquad\qquad + \varphi_2 \mathrm{rand}(0, a_2)(p_j^g(k) - x_j^i(k)) \end{cases} \tag{10}$$

where $i = 1, 2, \cdots, m$; $j = 1, 2, \cdots, n$. ω is the inertia weighting factor, $\varphi_1, \varphi_2 \in [0, +\infty)$ are acceleration constants, which controls the learning rate of the relative contributions of the individual cognitive component and the group social component. $rand(0, a_1)$ and $rand(0, a_2)$ are random numbers with uniform distribution in the range of values, a_1 and a_2 are corresponding control factors. The first part of the velocity update function is the velocity of the particle at the previous moment; the second part is the existing position of the individual particle compared to the optimal position ever experienced, indicating the cognitive ability of particles; and the third part indicates the information sharing among the particles. To prevent the velocity of the particle from being too large, set the threshold value of the velocity to $v_{\max}$.

IV. THE PROPOSED DESIGN STRATEGY OF FEEDBACK AND FEEDFORWARD

The force equalization controller is designed to suppress the adverse effects of disturbance on the system force fight and dynamic response, and the method of combining feedforward control and feedback control is used to compensate for the disturbance conditions in the system. The feedback control adopts fractional order PID control, and the controller parameters are optimized by particle swarm algorithm. Feed-forward control uses a torque observer to observe load disturbances and compensate for the current control with feed-forward gain, so as to achieve the control effect of small and strong control effect and strong robustness.

A. ERFORMANCE OF FITNESS FUNCTION

Since the error signal e(t) is constantly changing, an integral type of performance indicator is often used. A commonly used evaluation metric for optimal controllers is integrated time absolute error (ITAE), ITAE weighted the error, the weighting increased over time. The error signal can converge to zero as soon as possible. This characteristic makes it more suitable for the design of actual servo controller. The ITAE error integration criterion is defined as $J_{ITAE} = \int_0^\infty t\,|e(t)|\,dt$.

There is significant force fight in the system. By introducing force fight into the feedback loop in dynamic response, error of the system is compensated. The metric of the controller should take account both the position response and force fight. The fitness function of the specific index is shown in equation (11), where w_1, w_2 are weighting factors. Assigning parameter weights based on parameter magnitude: $w_1 = 1 \times 10^6$, $w_2 = 1$.

$$\begin{aligned} \mathrm{f(k)} = \mathrm{w_1} \int_0^{\mathrm{t}} (|\mathrm{x_a} - \mathrm{x_1}| + |\mathrm{x_a} - \mathrm{x_2}|) \cdot \mathrm{tdt} + \mathrm{w_2} \\ \times \int_0^{\mathrm{t}} |\mathrm{F_s} - \mathrm{F_m}| \cdot \mathrm{tdt} \end{aligned} \tag{11}$$

The essence of force equalization control is to reduce the output force difference between the actuators, which is largely related to the position deviation. To design the position synchronization control method to achieve the purpose of equalizing force fight and resisting system-related uncertainties and external disturbances.

B. PARICLE SWARM OPTIMIZATION OF FOPID PARAMRTERS

Firstly, initialization is performed to set the range of parameters such as: optimization parameter dimension, inertia factor, particle swarm size, acceleration constant, number of iterations, maximum velocity, and randomly generate the initial position matrix $[x_1, x_2, x_3, x_4, x_5] = [K_P, K_I, K_D, \lambda, \mu]$ and initial velocity in the range of values taken. Initial parameters of the particles are assigned to the controller, by running simulation models, the performance output is calculated for each iteration, position and velocity of these particles are continuously updated by iterating performance output until the optimal combination of parameters of the system is obtained. Optimal adaptation value reflects the degree of conformity to the fitness function as in equation (11), and the smaller the adaptation value means the smaller the error of the indicator function, that is, as the number of iterations increases, the system parameters are gradually optimized and the optimal adaptation value is smaller. As the number of iterations increases, the adaptation value shows a trapezoidal decreasing trend. The iterative process and the optimal individual adaptation values of successive generations are shown in Figure 6.

Based on the parameter range selected by the feedback PID controller, the upper and lower bounds of the value ranges of the P, I, and D parameters are set according to empirical values. Since the initial parameters of the particle swarm algorithm are generated randomly, the optimization parameters obtained from each iteration are not the same [31], the dichotomous idea in mathematics is used to correct the boundary conditions of the parameters. Generally, the order of fractional calculus is (0, 1), and according to experience, the order is too large to make the system less stable, while the order is too small to control the flexibility, the order of the controller is more stable between (0.4, 0.7). The parameters

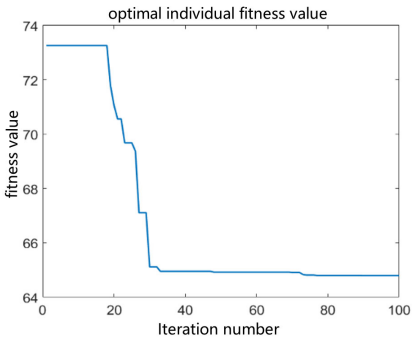

FIGURE 6. Optimization process of fitness.

TABLE 2. Combination of optimization parameters under different boundary conditions.

Parameters/Groups	P	I	D	λ	μ	ITAE
1	8.14×10^{-6}	8.0×10^{-7}	1.0×10^{-9}	1.2852	0.9165	95.45
2	9.34×10^{-6}	9.96×10^{-7}	9.69×10^{-9}	0.4813	0.5119	95.55
3	9.50×10^{-6}	1.0×10^{-6}	1×10^{-8}	0.4814	0.5289	101.72
4	1.50×10^{-5}	1.57×10^{-6}	8.59×10^{-8}	0.5	0.5065	86.21
5	1.96×10^{-5}	1.24×10^{-6}	7.03×10^{-8}	0.4540	0.5002	65.62

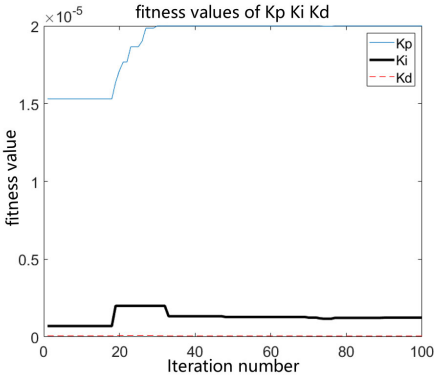

FIGURE 7. P, I, D optimization curve.

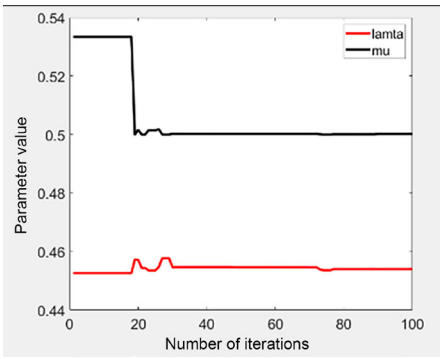

FIGURE 8. Fractional order optimization curve.

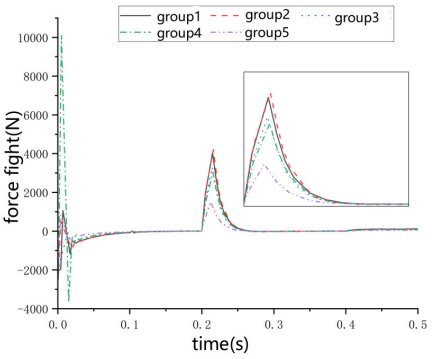

FIGURE 9. System response under different parameters.

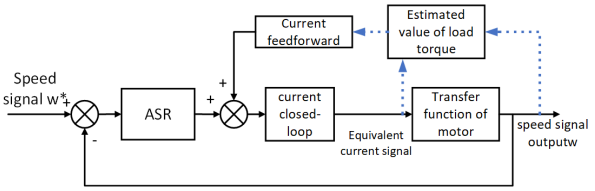

FIGURE 10. Feedforward control block diagram.

are set for 100 iterations, and the range of parameters are changed appropriately according to the parameter results after each iteration of the optimization search. Different sets of optimization-seeking parameters and the corresponding ITAE index values under different boundary conditions are shown in Table 2.

The upper and lower limits of parameters are determined by empirical parameters, P, I, and D ranges are taken as $(0, 2 \times 10^{-5})$, $(0, 2 \times 10^{-6})$, $(0, 1 \times 10^{-7})$, the range of integral and differential orders is (0.45,0.5), and (0.5, 0.55). The iterative optimization curves for P, I, and D parameters and the optimization curves for fractional order parameters are shown in Figure 7,8.

A comparison of the system force fight and position response for the above five sets of controller parameters is shown in Figure 9, which shows that the dynamic force fight is the smallest in the fifth set of parameters. So $P = 1.957 \times 10^{-5}$, $I = 1.24 \times 10^{-6}$, $D = 3 \times 10^{-8}$, $\lambda = 0.45402$, $\mu = 0.50019$ were chosen as the optimal parameters for the FOPID controller.

C. DESIGN OF FEEDFORWARD CURRENT COMPENSATION

The main idea of feedforward compensation for the motor is to construct an observer to observe the load disturbance and feed forward the observed disturbance value to the system for compensation as in fig10.

The sampling refresh frequency of the actual vector control algorithm is generally around 10 kHz to 20 kHz. It can be approximated that the load torque does not change during the unit sampling period $dT_L/dt = 0$.

According to equation (3), take the input $x = [\omega\ T_L]^T$, the controlled variable is $u = K_t i$, output variables is $y = \omega$,

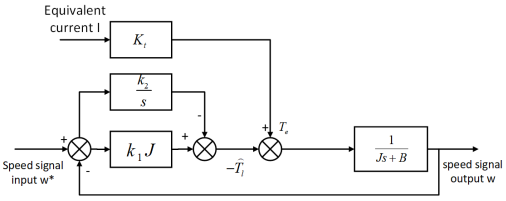

FIGURE 11. Diagram of the load torque step-down observer.

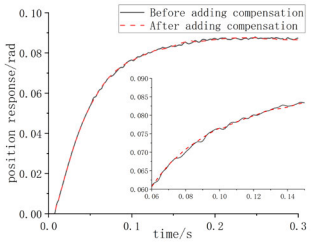

FIGURE 12. Comparison of system position response before and after adding feedforward compensation.

as in equation (12).

$$\begin{cases} \dfrac{dx}{dt} = Ax + Bu \\ y = Cx + D \end{cases} \tag{12}$$

where

$$A = \begin{bmatrix} -\dfrac{B}{J} & -\dfrac{1}{J} \\ 0 & 0 \end{bmatrix}, \quad B = \begin{bmatrix} \dfrac{1}{J} \\ 0 \end{bmatrix}, \; C = [\,1 \quad 0\,], \; D = 0.$$

Only the torque state variable needs to be observed, and the reduced-order state observer is designed as in Equation (13).

$$\begin{cases} \dfrac{dx}{dt} = A\hat{x} + Bu + K(y - \hat{y}) \\ y = C\hat{x} \end{cases} \tag{13}$$

The characteristic equation of the observer can be expressed as equation (14):

$$\hat{\omega} = \frac{T_e + (\omega - \hat{\omega})(k_1 J - \frac{k_2}{s})}{sJ + B} \tag{14}$$

The observed value of the load torque is obtained as equation (15):

$$\hat{T}_L = T_e - (sJ + B)\hat{\omega} = (\omega - \hat{\omega})(\frac{k_2}{s} - k_1 J) \tag{15}$$

The block diagram of the load torque step-down observer is as fig 11.

Select the conjugate pole k_1, k_2 as $(-100, \pm 75i)$ to achieve better dynamic response. In order to compare the robustness of the controller, the system position step response without compensation and with current compensation is compared, and the load torque is set as a random signal with an amplitude of 25N·m and a change frequency of 100Hz starting at 0.05s as in fig12.

The red curve is of adding external load compensation. Due to the disturbance of external load, the position response of the system without current feedforward has different degrees of fluctuation in the dynamic response process and the steady state where the steady-state error of the position command can reach 1.524%. After adding compensation, the maximum steady-state error is less than 0.733% of the position signal. The current loop feedforward compensation can speed up the response of the current loop to load torque changes, thus effectively enhancing the system's resistance to load disturbance.

V. CONTROL SYSTEM SIMULATION AND ANALYSIS

Considering the actual actuation system requirements, the maximum dynamic force dispute and static force dispute are used as the indicators for evaluating the force fight controller. In order to analyze the force fight response when the rudder surface is deflected to the limit position at maximum speed, the response of the system is set to be under step, triangle wave, and sine wave commands. Verify and analyze the response of the controller at different frequencies. Monte Carlo analysis was used to analyze and verify the overall robustness of the controller, and finally, the force fight data in the actual operation process of the experimental device was collected and added to the control system as a disturbance term to test the control effect of the controller on the actual force fight.

A. VERIFICATION OF STEP RESPONSE CONTROL EFFECT

To verify the effect of the controller on force fight, force fight response between PID controller, fractional-order PID, and FOPID with current feedforward (FO+IF) are in Figure 13. As shown in Figure 13(a) the dynamic force fight is greatly decreased after adding the fractional-order PID, and the static force fight drops to below 100 N. Qualitatively, through the FO+IF controller, the dynamic force fight has been reduced by 81N on the basis of FOPID.

The statistical analysis of the maximum dynamic force fight and static force fight in the system response process under different control methods is shown in Table 3. Assuming that the static force fight is the maximum allowable load force of the system, control the dynamic force fight within 20% of the maximum allowable load force, which is 10512.2N, and control the static force fight within 4% of the maximum allowable load force, which is 2102.44N.

The PID controller can control the maximum force fight within 19% before adding the controller, FOPID can regulate the maximum force fight within 2.3% before adding the controller. The PID controller controls the static force fight within 1.17%, FOPID and FO+IF controls the static force fight within 0.08%.

Compared with PID, FOPID and FO+IF controllers can better meet the requirements of force fight, and FO+IF behaves better in stability. Comparing FOPID and FO+IF controller, the response of the system to external disturbances becomes faster after adding current feedforward, and the peak force fight and static force fight are reduced. With current feedforward the system can better resist the impact

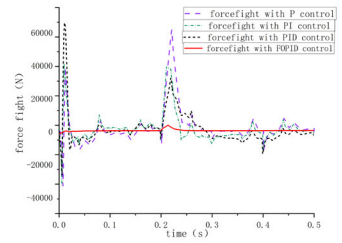

(a)Comparison of PID and FOPID

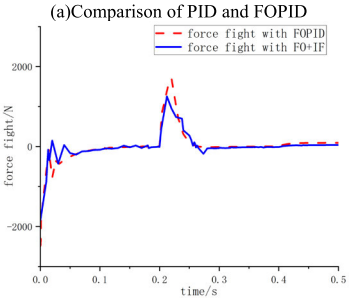

(b)Comparison of FOPID and FOPID with feedforward

FIGURE 13. Comparison of force fight under different controllers.

TABLE 3. Comparison of controllers' performance.

controller	Maximum of force fight	Static force fight
none	145861N	52561N
objective	10512.2N	2102.44N
P	61610N	7630N
PI	38847N	4372N
PID	27523N	3596N
FOPID	1708N	45N
FO+IF	1627N	42N

of sudden load torque change. In step response, the FO+IF control of feedforward and feedback has good performance in robustness of system and force fight.

B. TRIANGULAR WAVE DYNAMIC RESPONSE VERIFICATION

In order to better verify the dynamic response performance of the force equalization controller, the system is set at the maximum speed of the control surface, where position command in the model is a triangle wave deflection command with amplitude of 20°, T = 5s, and with the maximum torque load [32]. At the same time, the torque white noise disturbance is added. Under this condition, the control effects without equalization controller, FOPID and FO+IF force equalization methods are compared respectively. The results are shown in Figure 15.

Compared with the FOPID method, FO+IF has the following improvements: (1) The maximum force fight under the action of FOPID and FO+IF is 22475.2N and 6954.5N respectively, and position error reduced by 69%. (2) The static force fight generated by FOPID and FO+IF is 483.7N and

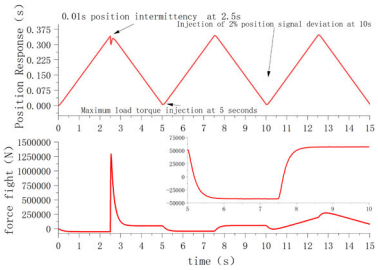

(a) Response without force equalization strategy

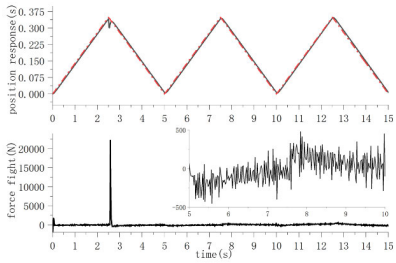

(b) Response with different FOPID force equalization strategy

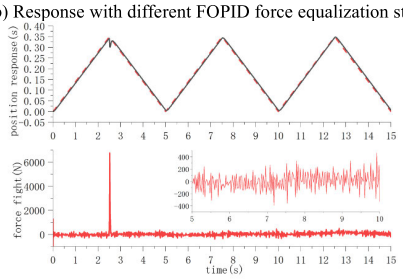

(c) Response with different FO+IF force equalization strategy

FIGURE 14. Force fight with different strategy.

261.3N respectively. (3) The control effect of load torque is better. From the overall control effect, FO+IF has a greater performance improvement than FOPID.

C. SINUSOIDAL RESPONSE VERIFICATION

The operating frequency of the controller is tested at 0∼5Hz. Force fight response of the system in different frequency range as 0.1∼5Hz is tested, the amplitude of the position signal is set as 20°. As the frequency of the position signal increases, force fight becomes worse, and the control effect of the force equalization controller becomes weaker. Comparing the control effects of force fight under different frequencies, as shown in Figure 15.

The black curve in Figure 15 shows the system force fight response without the force equalization controller. The red line and the blue line show force fight under the FOPID controller and FO+IF controller. With the increase of the command frequency, the peak value of the system force fight rises. Compared with FOPID controller, FO+IF controller has better anti-interference ability, improved control level of disturbance, less dynamic force fight, and higher static stability of the system. The maximum dynamic force fight of the two controllers at different frequencies are listed in Table 4. In each case, 20% of the maximum force fight

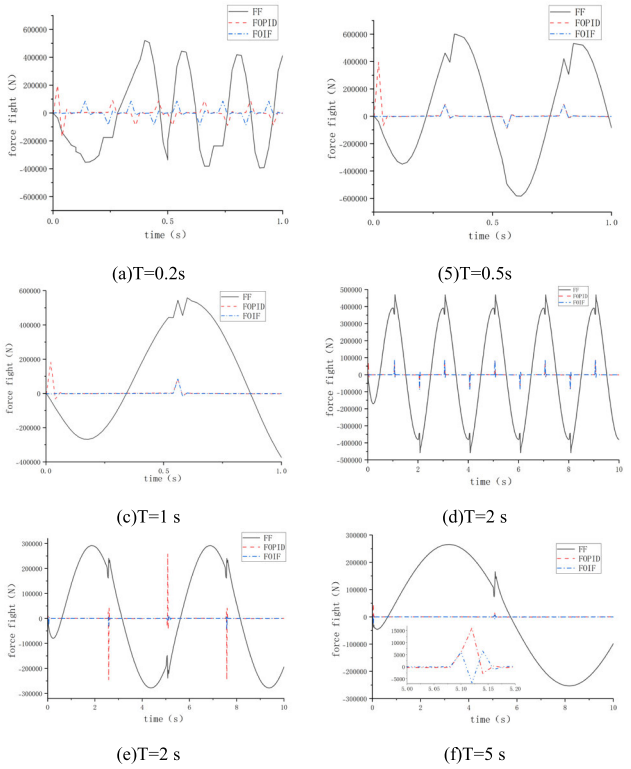

FIGURE 15. Force fight of different frequencies situations.

TABLE 4. Control effect of different controllers on maximum force fight.

Controller/time	none	control target	FOPID	FO+IF
T=0.2s	265430.6	53086.12	16058.5	6643.8
T=0.5s	291565.3	58313.06	258027.6	8948.1
T=1s	469134.2	93826.84	73340.3	84643.8
T=2s	558233.9	111646.8	181616.7	84917.2
T=5s	601848.6	120369.7	395713.1	85226.3
T=10s	520912.5	104182.5	198610.3	85764.2

of the system without the controller is set as the control target.

The control effect of FO+IF controller conforms to the maximum force fight requirement of the system. Compared with FOPID controller, dynamic force fight of the system increases slightly when T = 1s, and force fight convergence effect of FO+IF controller is better in other cases. When the operating frequency of the system exceeds 5Hz, the control effect of the controller on force fight with high frequency changes gradually decreases, and may even lead to the system instability.

D. ROBUSTNESS VERIFICATION

The Monte Carlo method is used to verify the robustness of control effect. The factors that have the greatest impact on the sensitivity of system force fight are mainly [16]: transmission

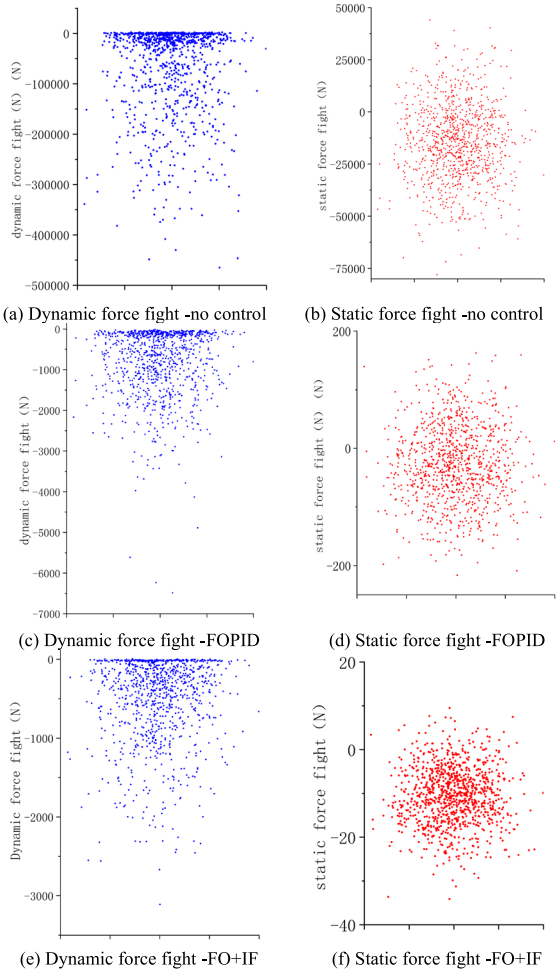

FIGURE 16. Distribution of system force fight scattering points.

TABLE 5. Comparison of different controllers on force fight.

controller	dynamic force fight	Static force fight
none	487264.5N	48241.1N
FOPID	6475.4N	158.8N
FO+IF	3208.3N	279.8N

efficiency deviation of reducer, position signal offset, position sensor delay, speed signal offset, and transmission clearance.

Set the parameters within the allowable range of variation, randomly select 1000 groups of parameters in the normal distribution, then conduct simulation experiments, record the maximum force fight and the steady-state value of force fight each time, and make a column scatter diagram, as shown in Figure 16.

Force fight distribution under various conditions is listed in Table 5.

In case of parameter fluctuation, the maximum dynamic force fight without controllers is 487264.5N,80% of force fight is distributed in the interval (0, 42580N). FOPID and

FO+IF control the maximum dynamic force fight within 1.334% and 0.657% of the initial force fight, respectively, and the control effect of FO+IF on the dynamic force fight induced by uncertain parameters is improved by about 50%. The efficiency of FO+IF in controlling the static force fight under the influence of uncertain parameters is improved by about 82.37%. It can be observed that FO+IF has good robustness and higher control accuracy in the case of parameter uptake.

During the controller design of future work, due to the introduction of the force equalization feedback loop, the cross-linking and coupling of the two channels increased, and the independence of the system decreased. The flight control system prohibits the existence of single point fault and common mode fault with redundant system, which has high requirements for the system independence. However, the controller saturation limit was not considered in the design of the balance scheme, In the case of serious force fight, the effect of the force equalization controller may be limited by the saturation limit. In the design of the force equalization controller in the future, more attention should be paid to the anti-saturation compensation of the controller [33] and other controller optimization ideas.

VI. CONCLUSION

In order to improve the performance of the force equalization controller in an active-active mode of dual redundant electromechanical actuation system, a method with fractional order PID control method based on PSO optimization and Current based feedforward control is adopted. Control effect of the proposed FOPID feedback and current feedforward method is validated by step response, triangular wave response and sinusoidal response simulation in the worst situation with parameters that have greatest impact on force fight. By performing a Monte Carlo analysis of parameter sensitivity, the experimental results show that the designed controller can enhance system robustness.

REFERENCES

[1] L. X. Chen, "Research on control strategy of electromechanical actuation servo system for more electric aircraft," Ph.D. dissertation, School Electron. Inf., Northwestern Polytechnical Univ., Xi'an, China, 2016, pp. 4–11.
[2] G. Dong, F. Wang, D. Meng, H. Chu, J. Hong, and B. Gao, "Modeling and control of ball-ramp electromechanical clutch actuator for in-wheel AMT of electric vehicles," *Mechanism Mach. Theory*, vol. 180, Feb. 2023, Art. no. 105129.
[3] K. Wei, J. Hu, J. Yao, H. Xing, and G. Le, "Fast terminal sliding mode control of neural networks for aeromechanical actuators," *Acta Aeronauticaet Astronautica Sinica*, vol. 42, no. 6, 2021, Art. no. 624540.
[4] J. Hu, Y. Sha, and J. Yao, "Dual neural networks based active fault-tolerant control for electromechanical systems with actuator and sensor failure," *Mech. Syst. Signal Process.*, vol. 182, Jan. 2023, Art. no. 109558.
[5] F. Y. Annaz, "Force equalisation in torque-summed electromechanical actuators," *Measurement*, vol. 156, May 2020, Art. no. 107600.
[6] D. A. DeFusco, "Hydraulic actuator force fight mitigation mechanism," USPTO Patent 20200003314, Defense Aerosp. Week, Sikorsky Aircr. Corp., Stratford, CT, USA, 2020.
[7] X. Jiang, W. Huang, Z. Hao, R. Cao, W. Li, Y. Sheng, and W. Jiang, "Redundant control system of dual-winding fault-tolerant permanent magnet motor," *Trans. China Electrotech. Soc.*, vol. 30, no. 6, pp. 22–29, Mar. 2015.
[8] D. Arriola and F. Thielecke, "Design of fault-tolerant control functions for a primary flight control system with electromechanical actuators," in *Proc. IEEE AUTOTESTCON*, Piscataway, NJ, USA, Nov. 2015, pp. 393–402.
[9] H. Wang, "Literature review on force fights and control methods of redundant actuator systems," *Aircr. Des.*, vol. 42, no. 3, pp. 35–38, 2022.
[10] P. Estival, R. Sehab, G. Krebs, and B. Barbedette, "Force fight and its elimination in a prototype of a redundant direct-drive avionic actuator," *Appl. Sci.*, vol. 10, no. 23, p. 8492, Nov. 2020.
[11] O. Cochoy, S. Hanke, and U. B. Carl, "Concepts for position and load control for hybrid actuation in primary flight controls," *Aerosp. Sci. Technol.*, vol. 11, nos. 2–3, pp. 194–201, Mar. 2007.
[12] Y. Fu, D. Fan, and Z. Li, "Static force equalization for dissimilar redundant actuator system," *J. Beijing Univ. Aeronaut. Astronaut.*, vol. 40, no. 11, pp. 1492–1499, Nov. 2014.
[13] D. Fan, Y. Fu, Y. Guo, and G. Zhou, "Dynamic force equalization for dissimilar redundant actuator system," *J. Beijing Univ. Aeronaut. Astronaut.*, vol. 41, no. 2, pp. 234–240, 2015.
[14] Y. Zhang and Z. Yuan, "Control strategy of Aileron's force-fight," *Int. J. Multimedia Ubiquitous Eng.*, vol. 9, no. 8, pp. 301–312, 2014.
[15] S. Ijaz, L. Yan, and M. T. Hamayun, "Fractional order modeling and control of dissimilar redundant actuating system used in large passenger aircraft," *Chin. J. Aeronaut.*, vol. 31, no. 5, pp. 1141–1152, May 2018.
[16] S. Ijaz, M. T. Hamayun, H. Anwaar, L. Yan, and M. K. Li, "LPV modeling and tracking control of dissimilar redundant actuation system for civil aircraft," *Int. J. Control, Autom. Syst.*, vol. 17, no. 3, pp. 705–715, Mar. 2019.
[17] Y. Xue and Z. Q. Yao, "A way to mitigate force-fight oscillation based on pressure and position compensation for fly-by-wire flight control systems," *Trans. Jpn. Soc. Aeronaut. Space Sci.*, vol. 63, no. 1, pp. 1–7, 2020.
[18] W. Ur Rehman, X. Wang, Y. Cheng, H. Chai, Z. Hameed, X. Wang, F. Saleem, and E. Lodhi, "Motion synchronization for the SHA/EMA hybrid actuation system by using an optimization algorithm," *Automatika*, vol. 62, nos. 3–4, pp. 503–512, Oct. 2021.
[19] Z. Bingul and O. Karahan, "Real-time trajectory tracking control of Stewart Platform using fractional order fuzzy PID controller optimized by particle swarm algorithm," *Ind. Robot*, vol. 49, no. 4, pp. 49–59, 2022.
[20] Y. He and J. Zhu, "The design of high-reliable dual-redundancy electromechanical actuator controller," in *Proc. World Congr. Intell. Control Automat.*, 2015, pp. 1439–1443.
[21] R. Tobias, E. Stumpf, and G. Weber, "An innovative all-active hybrid actuation system," in *Proc. AIAA Model. Simul. Technol. Conf.*, 2015, pp. 1–13.
[22] M. G. Antonelli, G. Bucci, F. Ciancetta, and E. Fiorucci, "Automatic test equipment for avionics electro-mechanical actuators (EMAs)," *Measurement*, vol. 57, pp. 71–84, Nov. 2014.
[23] H.-J. Lee, H.-D. Choi, and E.-S. Kang, "A study on the improvement of force fighting phenomenon in the redundant hydraulic servo actuators," *Aerosp. Eng. Technol.*, vol. 12, no. 1, pp. 54–63, 2013.
[24] E. S. Ali and S. M. Abd-Elazim, "Bacteria foraging optimization algorithm based load frequency controller for interconnected power system," *Int. J. Electr. Power Energy Syst.*, vol. 33, no. 3, pp. 633–638, Mar. 2011.
[25] X. Sun, D. Hou, and J. Yang, "Mechanism and sensitivity of force fight in dual redundant electromechanical actuators," *Acta Aeronautica et Astronautica Sinica*, vol. 44, no. 1, 2023, Art. no. 72766.
[26] H. Shu, Q. Tu, C. Jiang, H. Huang, and C. Zhu, "Global fast terminal sliding mode control based on fractional order differentiation for angular position synchronization control of PMSM," *IEEJ Trans. Electr. Electron. Eng.*, vol. 17, no. 8, pp. 1217–1227, Aug. 2022.
[27] J. Zhang, "Study on dual cylinder electro-hydraulic postion synchronization system based on compound fuzzy control," M.S. thesis, School Energy Sci. Eng., Harbin Inst. Technol Univ., Harbin, China, 2016, pp. 35–40.
[28] C. Y. Wang, "Study on fractional order PID controller parameter tuning methods and design," Jilin University, Jilin, China, Tech. Rep., 2013, pp. 29–38.
[29] D. Y. Xue, *Fractional Caculus and Fractional-Order Control*. Beijing, China: Science Press, 2018, pp. 115–126.
[30] S. Gao, L. Wang, and S. B. Chen, "An improved particle swarm optimization algorithm for fractional order PID parameter tuning," *Control Eng. China*, vol. 24, no. 10, pp. 2010–2015, 2017.

[31] A. M. Moghaddam, W. Kinsner, G. K. Costa, L. Kumar, K. Butt, and N. Sepehri, "FOPID control with parameter optimization for hydrostatically-actuated autonomous excavators," *IEEE Instrum. Meas. Mag.*, vol. 24, no. 2, pp. 109–117, Apr. 2021.
[32] Y. A. Xue, "Mitigation method for the electronic hydraulic servo actuators force fight oscillation," *Mech. Des. Res.*, vol. 37, nos. 53–58 and 67, pp. 1–7, 2021.
[33] R. Kowalski, "Force fight in parallel-redundant electro-mechanical actuation systems," in *Proc. Elelectric Aircraft*, Braunschweig, Germany, 2017, pp. 1–3.
[34] T. Li, T. Yang, Y. Cao, R. Xie, and X. Wang, "Disturbance-estimation based adaptive backstepping fault-tolerant synchronization control for a dual redundant hydraulic actuation system with internal leakage faults," *IEEE Access*, vol. 7, pp. 73106–73119, 2019.

JIANZHONG YANG received the B.S. and M.S. degrees from the Liaoning University of Engineering and Technology, in 1989 and 1992, respectively. He is currently a Professor with the College of Safety Science and Engineering, Civil Aviation University of China. His research interests include analysis of civil aircraft system safety and research on airworthiness certification and compliance verification technology of flight control systems.

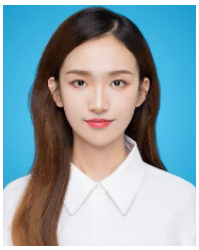

DONG HOU received the B.S. degree from the Civil Aviation University of China, in 2020, where she is currently pursuing the M.S. degree in aircraft airworthiness certification.

Her research interest includes control and simulation of the electrical mechanical systems.

XIAOZHE SUN received the B.S. degree in automation from Harbin Engineering University, Harbin, Heilongjiang, in 2004, and the Ph.D. degree from the College of Electrical Science and Automation, Beihang University, China.

Her research interests include fault-tolerant control of aircraft flight control actuation systems and safety analysis of civil aircraft flight control system architecture.

JINPENG ZUO received the B.S. degree from the Civil Aviation University of China, in 2021, where he is currently pursuing the M.S. degree in aircraft airworthiness certification. His research interests include controller design of the electrical mechanical systems.